# Improved deconvolution of bolus tracking data using wavelet thresholding

L. Willats[1], A. Connelly[2], F. Calamante[2]

[1]Institute of Child Health, University College London, London, UK, United Kingdom, [2]Brain Research Institute, Melbourne, Victoria, Australia

## Introduction

Deconvolution of bolus tracking data permits cerebral perfusion parameters to be estimated from the calculated tissue residue function $\check{R}(t)$ (1). When a global arterial input function (AIF) is used in the deconvolution, the shape of $\check{R}(t)$ reflects not only the tissue perfusion but also the distortion of the flow in the feeding vessels distal to where the AIF is measured. Delay and dispersion of the bolus due to abnormal vasculature distort $R(t)$ introducing an underestimation of cerebral blood flow (*CBF*), an overestimation of mean transit time (*MTT*), and errors in flow heterogeneity (FH (2)). Since these perfusion parameters are commonly used to predict regions of tissue at risk of infarction, differentiating the effects of distorted flow from a true perfusion abnormality is imperative for an accurate diagnosis. An important first step towards assessing the reliability of the perfusion parameters is to accurately characterise $\check{R}(t)$. Because the deconvolution problem is ill-posed, regularisation is needed for a stable solution. Maximum-likelihood expectation-maximisation (ML-EM) based deconvolution is able to recover all the constituent frequency components of $\check{R}(t)$, so can potentially reconstruct the correct shape (3,4). In this work, an oscillation index (*OI*) is used to regularise the ML-EM solution. Wavelet thresholding is subsequently employed to selectively remove the high frequency components thought to originate from noise (5,6). Combining the two techniques could potentially recover a $\check{R}(t)$ with less regularisation error and noise corruption compared with conventional deconvolution methods such as SVD (1). If the shape of $\check{R}(t)$ is accurately characterised, a dispersion index could be calculated and used in combination with the delay and *CBF* estimates to provide an improved interpretation of the data.

## Methods

The deconvolution was performed using ML-EM (3), with a maximum number of iterations, $n$ determined by an oscillation index (*OI*), defined as the sum over the size of each oscillation in the reconstruction $\check{R}^{[k]}$ at iteration, $k$, scaled by the *FWHM* of $\check{R}^{[k]}$. The *OI* is designed to prevent over iteration and consequent noise corruption of $\check{R}(t)$, whilst still recovering the high frequencies defining the less dispersed $\check{R}(t)$ (4).

The solution $\check{R}^{[n]}$, which is the first iteration for which $OI>0.025$, contains high frequency components, including those associated with amplified noise. A two level undecimated discrete wavelet transform of $\check{R}^{[n]}$ is performed using length four, minimum phase Daubechies' wavelet filters (5,6). The detail wavelet coefficients were thresholded to 10% of the maximum of the approximation. The inverse wavelet transform recovers the final estimation $\check{R}$.

The deconvolution process is performed twice using two different matrices ($\mathbf{A_1}$ and $\mathbf{A_2}$) to represent the AIF. The approximation used in $\mathbf{A_1}$, assumes that both $\check{R}(t)$ and AIF($t$) evolve linearly between sample points (1). This assumption is not appropriate if there is a discontinuity before the maximum of $\check{R}(t)$ (i.e. when the flow is delayed but not dispersed). In these circumstances, an alternative matrix $\mathbf{A_2}$, which assumes $\check{R}(t)$ is constant between sample points, allows a more accurate reconstruction (4). The most appropriate matrix is in practice selected using threshold criteria determined from simulations (see below).

This methodology was tested on simulated and patient data. For the simulations, AIF was modelled as a gamma-variate function with recirculation (1), and $\check{R}(t)$ as the dispersed exponential $\check{R}(t\text{-}t_{delay})=[exp(-(t\text{-}t_{delay})/\beta)\text{-}exp(-(t\text{-}t_{delay})/MTT)]/((\beta/MTT)\text{-}1)$,for delays $t_{delay}$ and dispersions $\beta$ (7). Tissue curves were simulated for a range of *CBF*, *MTT*, $t_{delay}$ and $\beta$. 100 different noisy tissue curves were generated at $SNR$=100 ($S_0/\sigma_{S0}$) for each parameter combination, and the means and standard deviations for each point in $\check{R}$ were evaluated. The patient data were acquired on a 1.5T Siemens Symphony scanner after injecting 0.15mmol/kg of Gd-DPTA using a GE-EPI sequence (TE/TR=47/1500ms), and denoising was performed using independent component analysis (ICA) (8).

The dispersion characteristics of $\check{R}$ were estimated using a dispersion index (*DI*) defined $DI=FWHM(\check{R})*RTM(\check{R})$, where *RTM* is the rise-to-maximum from baseline, included to distinguish between long *MTT* and dispersion. The delay was estimated from the length of the baseline, and the *CBF* estimated from the maximum of $\check{R}$.

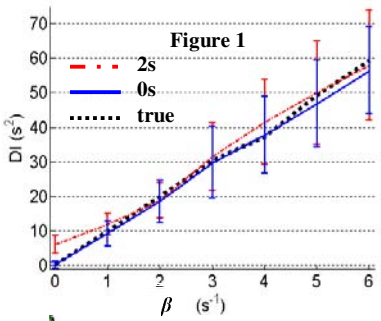


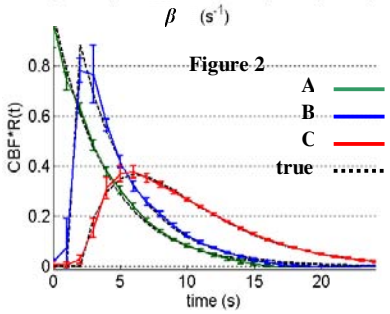


## Results

The simulations showed that matrix $\mathbf{A_2}$ (most suitable for delayed and non-dispersed flow) could be correctly selected where appropriate over matrix $\mathbf{A_1}$ using the combination of criteria $RTM_{A1}<2$ and $(CBF*DI)_{A2}<(CBF*DI)_{A1}$ and $(CBF)_{A2}<(CBF)_{A1}$ .For $t_{delay}$,=0-4s and $\beta$= 0-6s$^{-1}$ the success of the classification ranged 70-100%.

Figure 1 shows the mean *DI* (+/-1 standard deviation) measured from the 100 reconstructed $\check{R}$ (simulated with *CBF* =60ml/100g/min, *MTT*=4s) for $t_{delay}$ =0 and 2s and $\beta$=0-6s$^{-1}$. Each solid line and errorbar represents the measured *DI* for that delay. The dotted line is the *DI* calculated from the true $\check{R}(t)$ used to simulate the tissue. The approximately linear relationship between the simulated dispersion and the measured *DI* makes this parameter a useful for indicating the accuracy of perfusion estimates (greater dispersion leads to a greater distortion). Further simulations conducted with different flow parameters show that the slope increases as *MTT* increases.

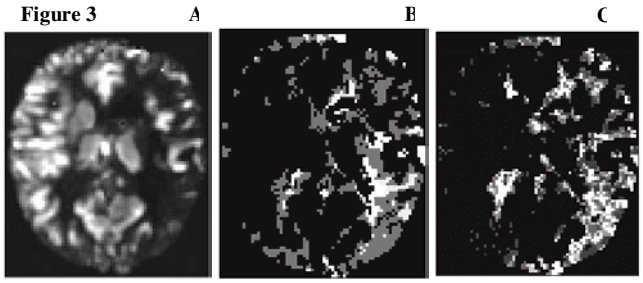


Figure 2 illustrates mean (+/-1 standard deviation) for simulations reconstructing $CBF*\check{R}(t)$ with A) $t_{delay}$=0s, $\beta$=0s$^{-1}$; B) $t_{delay}$=1.5s, $\beta$=0s$^{-1}$; C) $t_{delay}$=2s, $\beta$=4s$^{-1}$. The dotted lines show the true $\check{R}(t)$. A clear distinction can be made between the delayed and dispersed $\check{R}$, enabling a good estimation of delay and dispersion.

Figure 3 illustrates the results found for in vivo data from a patient with left middle cerebral artery (MCA) stenosis. The maps were created using an AIF measured in the contra-lateral MCA. A) *CBF*, B) $t_{delay}$, C) *DI*. Regions corresponding to low *CBF* estimates are found to have larger delay and dispersion, with the consequence that the *CBF* map would exaggerate any perfusion deficit in these regions.

## Discussion

An accurate characterisation of $\check{R}(t)$ is important for assessing tissue viability. In patients with vascular abnormalities, interpreting the *CBF* maps independently of the shape of $\check{R}(t)$ may lead to a misclassification of ischaemic tissue. Combining oscillation constrained ML-EM and wavelet analysis is shown to be an effective way to simultaneously minimise noise whilst preventing distortion of $\check{R}$ due to over regularisation, enabling delay and dispersion to be estimated which may assist the interpretation of *CBF*.

The combined ML-EM-wavelet approach to calculating $\check{R}(t)$ utilises the same concept as the *point-wise* stopping criteria in modified ML-EM (mML-EM) (4), designed to selectively recover the high frequency components associated with $\check{R}(t)$ itself whilst suppressing those associated with noise. Whereas the criteria used in mML-EM must be adjusted for various scanning parameters, the wavelet thresholding approach provides a universal criterion for all data.

## References

(1) Østergaard et al. (1996) MRM 36:715. (2) Østergaard et al. (1999) JCBFM 19:690. (3) Vonken et al. (1999) MRM 41:343. (4) Willats et al. (2005) ISMRM 41. (5) Mallat (1989) IEEE 2:674. (6) Wirestam et al. (2005) MAGMA. (7) Calamante et al. (2000) MRM 44:466. (8) Calamante et al. (2004) MRM 52:789.